The Effect of Fluoro Substitution upon the β-Hairpin Fold of a β-Tetrapeptide in Methanol

by **Stephan Bachmann**[a]), **Bernhard Jaun**[b]), **Wilfred F. van Gunsteren***[a]), and **Dongqi Wang***[a])

[a]) Laboratory of Physical Chemistry, Swiss Federal Institute of Technology, ETH, CH-8093 Zürich (e-mail: wfvgn@igc.phys.chem.ethz.ch, wangd@igc.phys.chem.ethz.ch)

[b]) Laboratory of Organic Chemistry, Swiss Federal Institute of Technology, ETH, CH-8093 Zürich

The importance of β-peptides lies in their ability to mimic the conformational behavior of α-peptides, even with a much shorter chain length, and in their resistance to proteases. To investigate the effect of substitution of β-peptides on their dominant fold, we have carried out a molecular-dynamics (MD) simulation study of two tetrapeptides, Ac-(2*R*,3*S*)-$\beta^{2,3}$hVal(αMe)-(2*S*)-β^{2}hPhe-(*R*)-β^{3}hLys-(2*R*,3*S*)-$\beta^{2,3}$-Ala(αMe)-NH_2, differing in the substitution at the C_α of Phe2 (pepF with F, and pepH with H). Three simulations, unrestrained (UNRES), using ^3J-coupling biasing with local elevation in combination with either instantaneous (INS) or time-averaging (AVE) NOE distance restraining, were carried out for each peptide. In the unrestrained simulations, we find three (pepF) and two (pepH) NOE distance bound violations of maximally 0.22 nm that involve the terminal residues. The restrained simulations match both the NOE distance bounds and ^3J-values derived from experiment. The fluorinated peptide shows a slightly larger conformational variability than the non-fluorinated one.

Introduction. – The many particular roles that proteins play in biological processes derive from the particular conformational properties of their constituents, α-amino acids linked by peptidic bonds. This led to the question whether other building blocks of polymers and linkages between them could be formed or synthesized that possess conformational properties similar to those of α-polypeptides. Nowadays, a plethora of so-called peptoids is known [1]. A particular class of peptoids are the β-amino acids, which possess an additional C-atom in the backbone compared to the natural α-amino acids [2][3]. β-Peptides combine the ability to permeate a cell membrane or to attach to a protein receptor with a strong resistance to proteases [4].

Previous experimental studies [5–12] revealed different secondary structures, helices and hairpins, depending on the amino acid sequence and side-chain substitution of the β-amino acids. This led to the question which interactions or topological features are responsible for the dominance of a particular fold. Folding of peptides can be influenced by H-bonding, hydrophobic interactions, *Van der Waals* and electrostatic interactions, solvation, and backbone conformational entropy [13]. Compared to α-peptides, β-peptides display a broader range of dominant secondary structures and may adopt stable secondary structure with as few as four residues [5][14][15]. This and the fact that most experimental studies of β-peptides included MeOH as solvent made them ideal molecules to study the process of secondary-structure formation computationally. Due to its lower density of interaction sites, MeOH models can be simulated four times more efficiently than H_2O models.

The effect of different substitutions on β-peptides on the formation of helical structure has been addressed in a few computational studies [16–18]. With a second aliphatic C-atom in the backbone, β-peptides have one more rotatable backbone torsional angle (θ) than the two (φ and ψ) of an α-amino acid, and it has four instead of two backbone H-atoms that can be substituted. Due to the steric interaction between side chains and backbone, the folding of β-peptides is highly dependent on the substitution pattern. However, the effect of the substitution pattern for β-peptides that adopt predominantly hairpin secondary structure, such as the ten-membered hairpin turn, is not well studied computationally.

Recently, an experimental study has been reported that addresses this issue [19]. Two tetrapeptides, Ac-(2*R*,3*S*)-$\beta^{2,3}$hVal(αMe)-(2*S*)-β^2hPhe-(*R*)-β^3hLys-(2*R*,3*S*)-$\beta^{2,3}$-Ala(αMe)-NH_2, and its analog in which the β^2hPhe residue bears a F-atom at C_α, were synthesized and subjected to NMR study. The experiment did not detect a measurable influence of the F_α-atom on the dominant hairpin fold, partly due to a lack of NOEs to define the local conformation in the turn. Both peptides show the same structural features in MeOH: a hairpin turn in the middle of the chain with a ten-membered H-bonded ring. To obtain a more detailed picture of the conformational space that is accessible to these peptides at room temperature and pressure, we carried out a molecular-dynamics (MD) simulation study based on the observed NOE and $^3J(H_N,H_\beta)$ NMR data [19] for the fluorinated peptide **2** and the non-fluorinated peptide **3** (*Fig. 1*).

Computational Details. – The two peptides, pepF, the fluorinated peptide **2** of [19], and pepH, the non-fluorinated peptide **3** [19], and solvent were modeled using the

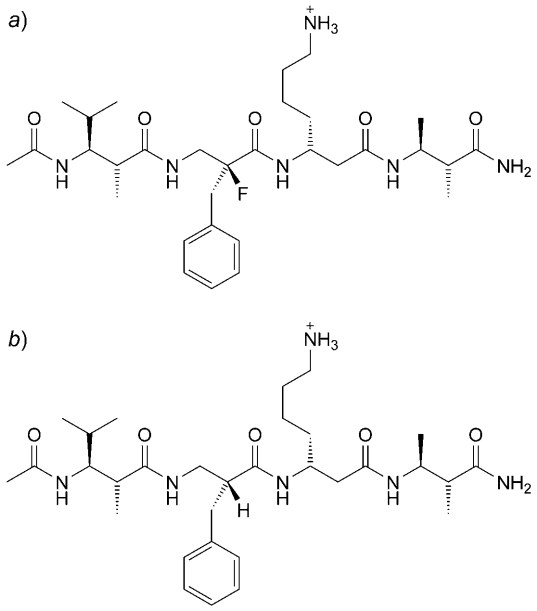

Fig. 1. *Peptides pepF* (*a*; fluorinated peptide **2** [19]) *and pepH* (*b*; non-fluorinated peptide **3** [19])

program GROMOS [20][21] and the GROMOS force field 53A6 [22]. The force-field parameters involving the F-atom were taken from [23]. The MeOH molecules were modeled using a rigid three-site model [20][24]. Aliphatic CH_n groups of the solute and the solvent were treated as united atoms. The Lys side chain was protonated and a Cl^- anion was added to neutralize the system. One of the NMR model structures obtained through single-structure refinement [19] was taken as initial structure for the MD simulation. The system was simulated in a cubic box using periodic boundary conditions with an initial box length of 5.5 nm, and there are 2468 MeOH molecules in the simulations of pepH and 2464 in the simulations of pepF. All bond lengths were constrained using the SHAKE algorithm [25] with a relatively geometric tolerance of 10^{-4} allowing for a time step of 2 fs. Long-range electrostatic interactions were handled with a triple-range cut-off scheme [20][21] with cut-off radii of 0.8 nm (interaction updates every timestep) and 1.4 nm (interaction updates every five timesteps). The mean effect of omitted electrostatic interactions beyond the long-range cut-off distance (1.4 nm) was accounted for by the inclusion of a *Barker–Watts* reaction-field force [26][27] using a dielectric permittivity of $\varepsilon_{rf} = 19$ [24]. The weak-coupling method [28] was used for keeping the temperature (300 K) and pressure (1 atm) constant, using coupling times $\tau_T = 0.1$ ps, $\tau_P = 0.5$ ps, and an isothermal compressibility of 4.575×10^{-4} kJ^{-1} mol nm^3. Both the fluorinated and non-fluorinated peptide were equilibrated for 1 ns. Apart from unrestrained or unbiased simulations, three different types of restraining or biasing procedures that restrain or bias the simulations towards reproduction of measured properties were applied:

i) so-called local-elevation (LE) biasing of ^3J couplings (J-LE) [29][30],

ii) instantaneous distance restraining of NOE atom–atom pairs (NOE-INS) [31], and

iii) time-averaged distance restraining of NOE atom–atom pairs (NOE-TAV) [32].

The conformations of the peptide were then sampled in three simulations: unrestrained (UNRES), using ^3J-coupling biasing through local elevation in combination with instantaneous NOE restraints (INS), and using ^3J-coupling biasing in combination with time-averaging NOE restraints (AVE). The primary experimental data [19], used for the ^3J-coupling biasing and NOE distance restraining, include 28 (fluorinated, Table S1[1])) and 29 (non-fluorinated, Table S2[1])) NOE distance bounds, and five (fluorinated) and three (non-fluorinated) $^3J(H_\beta,H_N)$ couplings (see *Table 1*). The parameters for the local-elevation biasing towards the experimental ^3J-coupling values were $k_{LE} = 1 \times 10^{-3}$ kJ mol^{-1} Hz^{-4}, $N_{LE} = 36$, and $\tau_{LE} = 5$ ps [30]. The parameters for distance restraining were $k_{dc} = 1000$ kJ mol^{-1} nm^{-2} for instantaneous and $k_{dc} =$ 1000 kJ mol^{-1} nm^{-2} and $\tau_{dc} = 5$ ps for time-averaging restraining [32]. The unrestrained simulations covered 100 ns, and the other simulations 30 ns, because their sampling is expected to converge faster due to the biasing or restraining forces.

The analysis of the trajectories is similar to that in described [33]. The various averages were also calculated using the NMR model structures (30 for pepF and 29 for pepH) that had been obtained by single-structure refinement using simulated

---

[1]) *Supplementary Material* regarding NOE distance bounds of peptides pepF and pepH is available from the authors upon request.

annealing [19]. The criterion used in the H-bond analysis is 0.27 nm as upper bound for the H···A (acceptor) distance and 135° as lower bound of the D···H···A angle (D: donor). A conformational clustering analysis [34] was performed for the trajectory structures at 10-ps intervals using a backbone (N,CB, CA, C, except for the Ac and NH_2 groups) atom-positional root-mean-square difference (rmsd) criterion of 0.08 nm. Three combined conformational clustering analyses were carried out for the trajectory structures combining the AVE simulations and the NMR model structures of pepH, of pepF, and combining the AVE simulations of pepH and pepF, using 15000 structures from each trajectory, or 500 or 517 copies of each of the 30 or 29 NMR model structures, leading to a total number of 30000 structures in each analysis. The H···H distances involving aliphatic H-atoms were calculated by defining virtual (CH_1), prochiral (stereospecific CH_2), and pseudo (non-stereospecific CH_2 and CH_3) atom positions, and the NOE distance bounds involving pseudo-atoms were modified to include pseudo-atom distance bound corrections [35]. ^3J-Coupling constants were obtained using the *Karplus* relation [36][37], with the parameters a, b, c being 6.4, −1.4, and 1.9 Hz, respectively [38].

Results and Discussion. – The calculated NOE distance bound violations are shown in *Fig. 2* and specified in Tables S1 and S2[1]), and the calculated ^3J couplings are given in

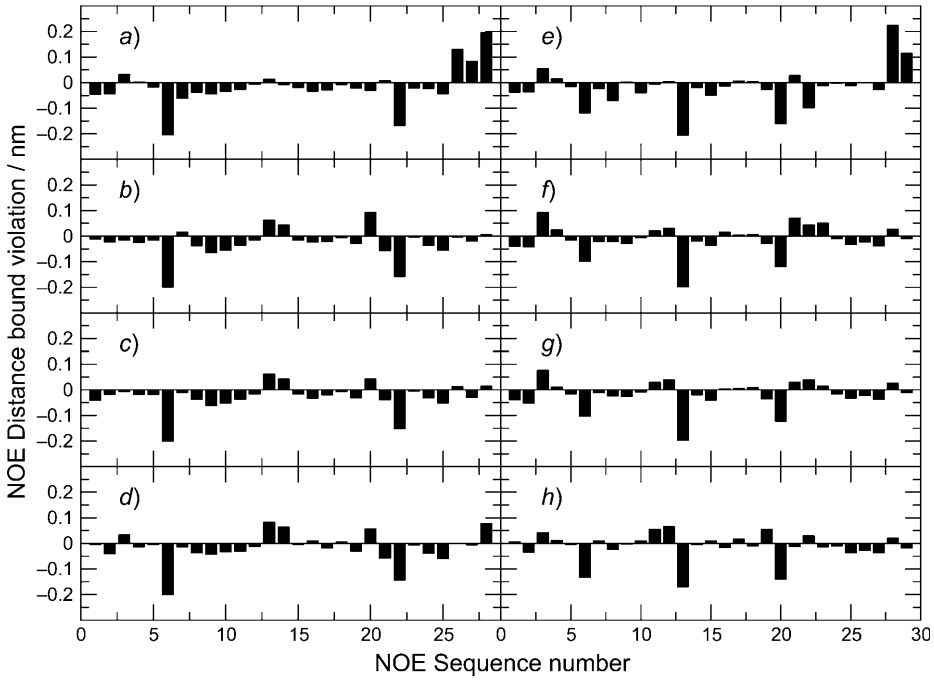

Fig. 2. *NOE Distance bound violations in pepF* (left column) *and pepH* (right column) *from simulations UNRES* (*a* and *e*), *INS* (*b* and *f*), *AVE* (*c* and *g*), *and the set of 30 or 29 NMR model structures* [19] (*d* and *h*). The 28 distances for pepF and the 29 for pepH are obtained by r^{-6} averaging. For further information, see caption of *Table 1*.

Table 1. The ^3J couplings in the unrestrained simulation (UNRES) do not deviate much from the experimental values. The largest deviation is 1.4 Hz. The same conclusion holds for the NMR model structures (NMR) with a largest deviation of 1.1 Hz. In the unrestrained MD simulations (UNRES) of both peptides, a few NOE distance bounds are violated, three for PepF and two for PepH. These violations involve atoms in the terminal residues: Val1 : H_α-Ala4 : H_β, Phe2 : HN-Ala4 : H_β, and Val1 : HN-Ala4 : H_β. Application of ^3J-coupling biasing and NOE distance restraining, either through instantaneous (INS) or through time-averaging (AVE) restraints, does, as expected, improve the agreement with the measured data.

Table 1. $^3J(H_N,H_\beta)$ *Coupling Constants* [Hz] *Averaged over the Different Simulations and the Set of 30 or 29 NMR Model Structures for Both Peptides Calculated with the* Karplus *Relation*

Peptide	Description	Exp [19]	UNRES[a])	INS[b])	AVE[c])	NMR model[d]) [19]
pepF	$\beta^{2,3}$hVal(αMe)	10.2	9.4	9.3	9.3	9.1
	β^2hPhe	7.8	6.4	7.9	7.7	8.0
	β^2hPhe	4.4	5.7	4.9	4.9	4.2
	β^3hLys	9.0	9.1	9.5	9.5	9.5
	$\beta^{2,3}$Ala(αMe)	8.7	9.0	9.4	9.4	8.9
pepH	$\beta^{2,3}$hVal(αMe)	10.3	9.3	9.4	9.4	9.3
	β^3hLys	8.8	9.1	9.5	9.4	7.9
	$\beta^{2,3}$hAla(αMe)	8.9	8.9	9.4	9.5	8.9

[a]) UNRES: unrestrained MD simulations. [b]) INS: MD simulations with local-elevation biasing towards experimental ^3J values in combination with instantaneous NOE distance restraining. [c]) AVE: *idem*, but with time-averaging instead of instantaneous NOE distance restraining. [d]) NMR: the set of NMR model structures obtained by single-structure refinement [19].

To characterize the ensembles of structures generated, the H-bonds with a population more than 10% are tabulated in *Table 2*, and *Fig. 3* shows the H-bond donors and acceptors. The set of NMR model structures did not contain any H-bond. The simulations displayed three H-bonds, Phe2 : HN-Lys3 : C=O, Ala4 : HN-Val1 : C=O, and Phe2 : HN-Ala4 : C=O, in both pepF and pepH, while two H-bonds, Val1 : HN-Phe2 : C=O and Val1 : HN-Ala4 : C=O, were only observed for pepF, and two other H-bonds, Lys3 : HN-Ala1 : C=O and Ala4 : HNT-Phe2 : C=O, only for pepH. The H-bond between Phe2 : HN and Lys3 : C=O closes the hairpin turn with a ten-membered H-bonded ring. In all simulations, its presence is less than 30%. Regarding the much higher population of the hairpin turn conformation sampled in the simulations (*Fig. 4*), the ten-membered ring-forming H-bond is not likely to be the driving force for the formation of the hairpin turn. This is consistent with a recent investigation of two α/β-mixed peptides [39].

In the restrained simulations, the presence of H-bonds is increased. In pepH, the Ala4 : HN-Val1 : C=O H-bond is replaced by the Phe2 : HN-Ala4 : C=O one. From the conformational clustering analysis results displayed in *Fig. 4*, we see that distance restraining enhances the population of the most populated clusters, for instantaneous restraining more than for time-averaging restraining.

Table 2. *Occurrence* [%] *of H-Bonds* (residue numbers and atoms)[a]) *That Are Populated More Than 10%*

Peptide	Donor	Acceptor	UNRES	INS	AVE	NMR
pepF	2-HN	3-C=O	17	27	28	–
	4-HN	1-C=O	11	–	–	–
	1-HN	2-C=O	–	–	22	–
	1-HN	4-C=O	–	29	12	–
	2-HN	4-C=O	–	14	14	–
pepH	2-HN	3-C=O	14	22	24	–
	4-HN	1-C=O	19	–	–	–
	2-HN	4-C=O	–	59	39	–
	3-HN	1-C=O	15	–	–	–
	4-HNT	2-C=O	16	–	–	–

[a]) For further explanation, see caption of *Table 1*.

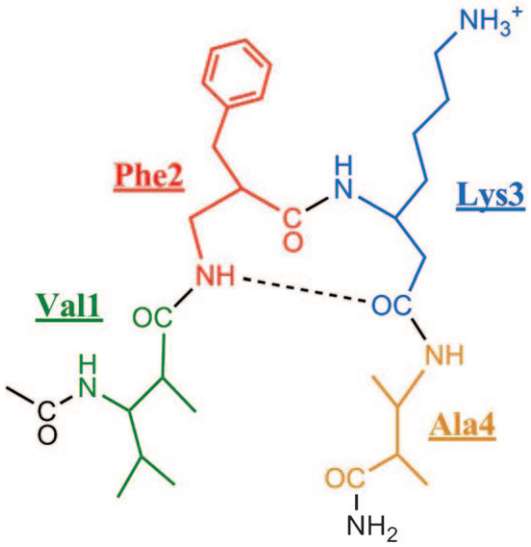

Fig. 3. *A schematic elucidation of the hairpin turn of the peptide pepH, and the H-bond donors and acceptors.* The H-bond that closes a ten-membered ring at the hairpin is shown with a dashed line which bridges the Phe2 : HN and Lys3 : C=O atoms.

The central structures of the most populated clusters have clear hairpin character. In all of the three simulations, the most populated cluster of pepF has a smaller population than the one of pepH (see also *Table 3*). In agreement with the conclusions of [19], the conformational ensemble of pepF is broader than that of pepH.

The combined clustering analysis of the trajectory structures in the AVE simulations of PepF and PepH, with the set of NMR model structures, shows that the simulations sample a more extended conformational space than spanned by the 30

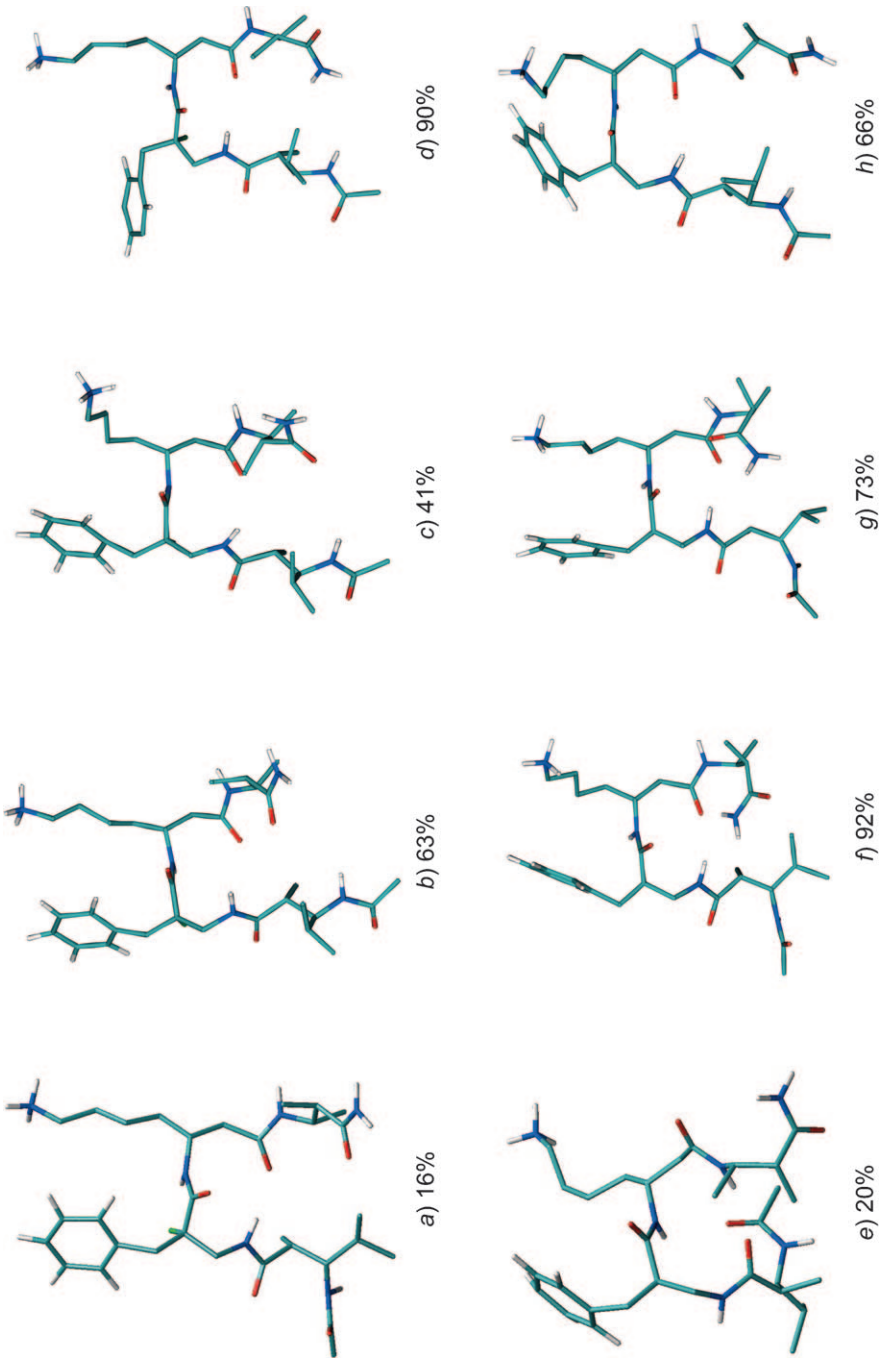

Fig. 4. *Central structures of the most populated clusters in the simulations of pepF* (*a*–*d*) *and pepH* (*e*–*h*) *and the set of NMR model structures* (*d*, *h*) [19]. *a*), *e*) UNRES; *b*), *f*) INS; *c*), *g*) AVS.

or 29 NMR model structures (*Fig. 5*,*a* and *b*). PepF shows more conformational variability than pepH (*Fig. 5*,*c*).

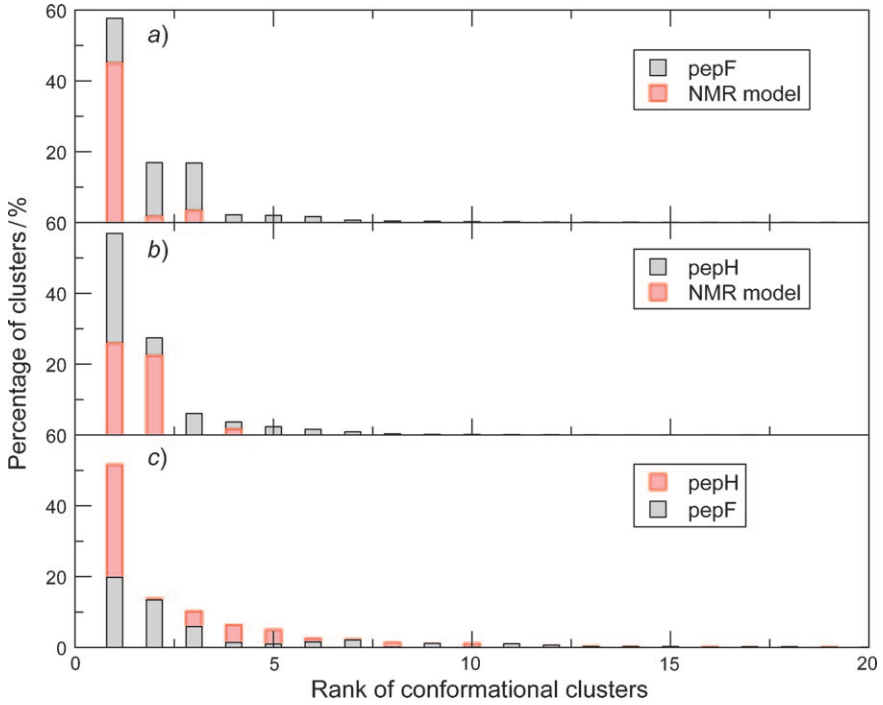

Fig. 5. *Conformational clustering analysis by combining the set of NMR model structures with the trajectories of the AVE simulations of pepH or pepF, and by combining the AVE trajectories of pepH and pepF*

Table 3. *Population* [%] *of the First Five Conformational Clusters*

Simulation		Cluster				
		1	2	3	4	5
pepF	UNRES	16	13	10	4	4
	INS	63	28	3	2	2
	AVE	41	27	10	6	5
pepH	UNRES	20	14	10	8	5
	INS	92	3	2	1	1
	AVE	73	12	5	4	2

The influence of the F-substitution on the distribution of the ψ torsional angle value of Phe2 and of the φ torsional angle value of the Lys3 is reflected in *Figs. 6–9*. These two torsional angles are in the hairpin turn. In the unrestrained simulations (*Fig. 6*), the Phe2 : ψ is populating two regions centered at $-60°$ and $120°$. The population at $\psi = -60°$ reflects unfolding of the hairpin turn. Comparing the populations of the Phe2 : ψ for pepH and pepF, it becomes clear that fluorination stabilizes the hairpin turn, *i.e.*, the

population of conformation $-60°$ of Phe2 : ψ is significantly reduced in pepF compared to pepH. Application of the restraints has the same effect: the distribution of Lys3 : φ becomes narrower at 120° (*Figs. 7* and *8*), and that of Phe2 : ψ shows peaks at 120° (pepH) or 80°, and 130° (pepF), in accord with the NMR model structures (*Fig. 9*). For the other torsional angles of the central residues Phe2 and Lys3, in both peptides the restrained simulations (INS, AVE) produce a narrower or more neat distribution than the UNRES simulations. For example, in the UNRES simulations, the θ angle distribution of the two residues shows three peaks (Phe2, centered at 60°, 180°, and $-60°$) or two peaks (Lys3, centered at 180°, and $-60°$) angles. These change to two (Phe2, centered at 50°, and $-60°$) and one (Lys3, $-60°$) peak in the restrained simulations. The bifurcation of the distributions of the torsional angles of Phe2 is more apparent in pepF than in pepH, showing the influence of fluorination.

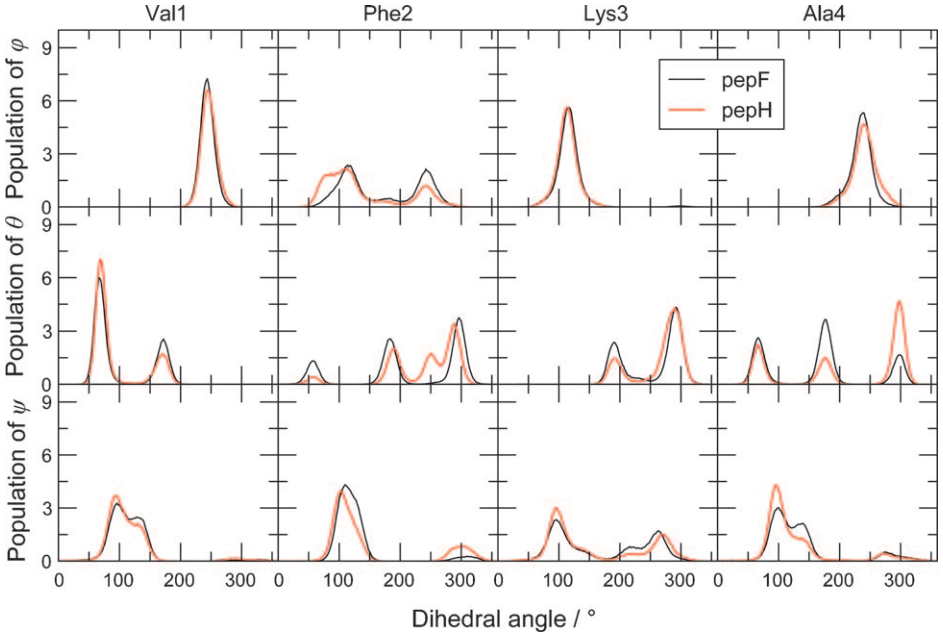

Fig. 6. *Population analysis of the three torsional angles* (φ, θ, and ψ) *of the four residues in the unrestrained simulations* (UNRES) *of pepF* (black) *and pepH* (red)

Conclusions. – In this study, we have used MD simulations with the GROMOS 53A6 force field to investigate the influence of fluorination at the C_α-atom of Phe2 of a β-tetrapeptide on its dominant hairpin-like secondary structure. Three simulations have been performed for the fluorinated (pepF) and the non-fluorinated (pepH) peptides, including an unrestrained simulation, and two simulations that use recorded NMR data as restraints.

The unrestrained MD simulations disagree with a few experimental data, but do contain a hairpin structure as the most populated conformation. The conformational clustering analysis indicates that, in the unrestrained simulations, there are a substantial

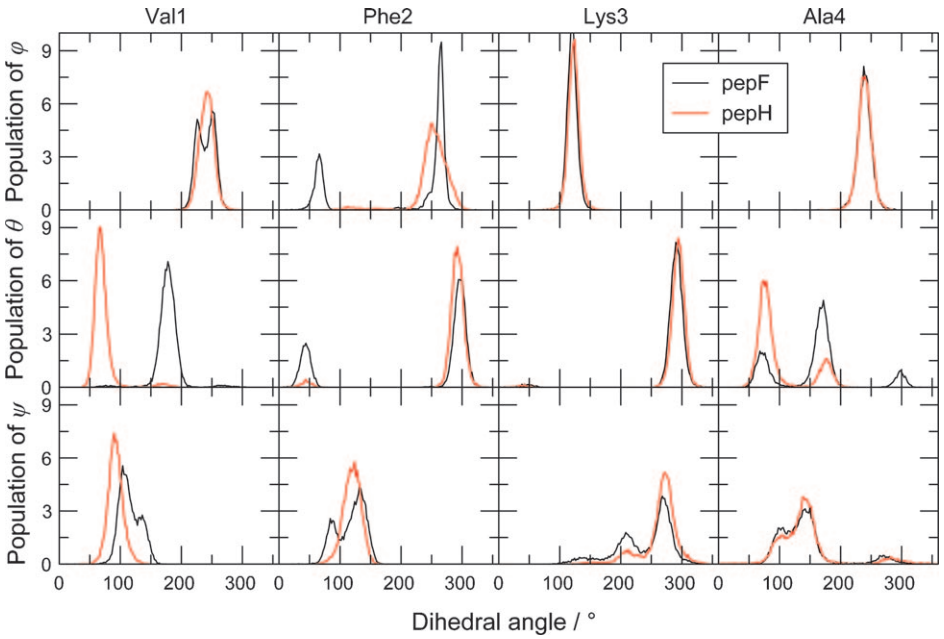

Fig. 7. *Population analysis of the three torsional angles* (φ, θ, and ψ) *of the four residues in the INS simulations of pepF* (black) *and pepH* (red)

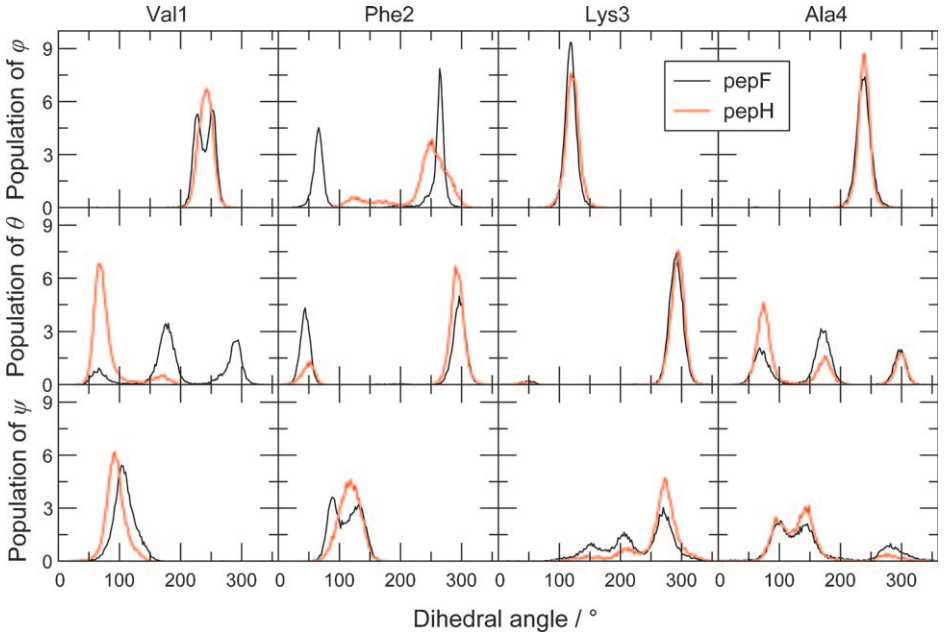

Fig. 8. *Population analysis of the three torsional angles* (φ, θ, and ψ) *of the four residues in the AVE simulations of pepF* (black) *and pepH* (red)

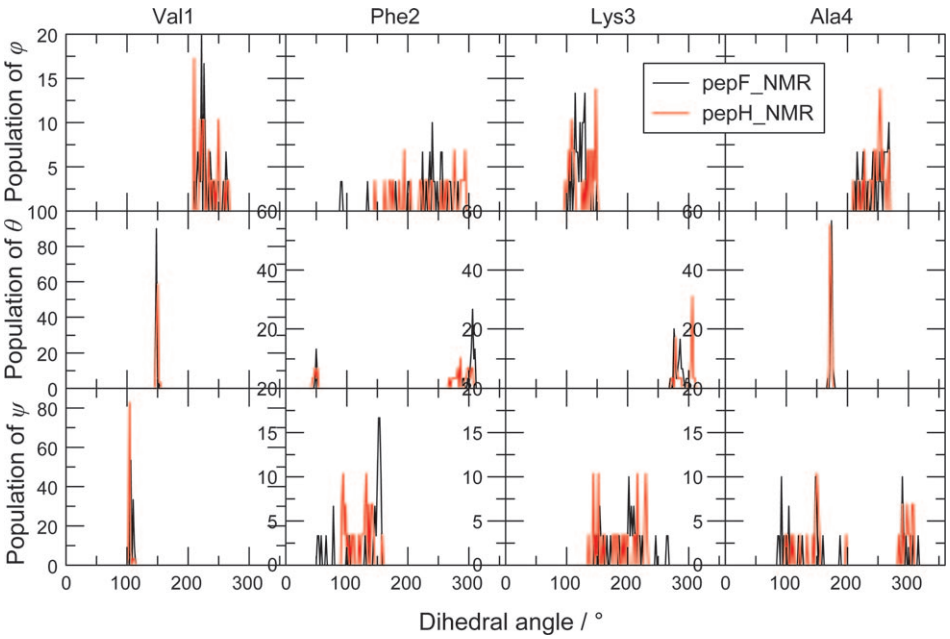

Fig. 9. *Population analysis of the three torsional angles* (φ, θ, and ψ) *of the four residues in the NMR model structures* [19] *of pepF* (black) *and pepH* (red)

number of conformations for which the hairpin turn opened up, reflected also by the population of the torsional angle Phe2 : ψ at $-60°$. Biasing of the simulations using both ^3J-coupling values and NOE distance bounds enhances the intra-solute H-bonding and enhances the population of the hairpin turn. According to our simulations, the fluorinated peptide shows a slightly larger conformational variability than the non-fluorinated one. As an electron-withdrawing atom, F may change the local electronic structure of Phe2, allowing for a more extended sampling of conformational space.

The authors thank the *Swiss National Science Foundation*, grant No. 200021-121913, and its *National Competence Center for Research* (*NCCR*) *in Structural Biology*, and the *European Research Council*, grant No. 228076, for financial support.

REFERENCES

[1] 'Foldamers: Structure, Properties, and Applications', Eds. I. Huc, S. Hecht, Wiley-VCH, Weinheim, 2007.
[2] D. Seebach, S. Abele, J. V. Schreiber, B. Martinoni, A. K. Nussbaum, H. Schild, H. Schulz, H. Hennecke, R. Woessner, F. Bitsch, *Chimia* **1998**, *52*, 734.
[3] S. H. Gellman, *Acc. Chem. Res.* **1998**, *31*, 173.
[4] D. Seebach, A. K. Beck, D. J. Bierbaum, *Chem. Biodiversity* **2004**, *1*, 1111.
[5] R. P. Cheng, S. H. Gellman, W. F. DeGrado, *Chem. Rev.* **2001**, *101*, 3219.
[6] A. Hayen, M. A. Schmitt, F. N. Ngassa, K. A. Thomasson, S. H. Gellman, *Angew. Chem., Int. Ed.* **2004**, *43*, 505.
[7] S. De Pol, C. Zorn, C. D. Klein, O. Zerbe, O. Reiser, *Angew. Chem., Int. Ed.* **2004**, *43*, 511.

[8] R. S. Roy, I. L. Karle, S. Raghothama, P. Balaram, *Proc. Natl. Acad. Sci. U.S.A.* **2004**, *101*, 16478.
[9] M. A. Schmitt, S. H. Choi, I. A. Guzei, S. H. Gellman, *J. Am. Chem. Soc.* **2005**, *127*, 13130.
[10] K. Ananda, P. G. Vasudev, A. Sengupta, K. M. P. Raja, N. Shamala, P. Balaram, *J. Am. Chem. Soc.* **2005**, *127*, 16668.
[11] G. V. M. Sharma, P. Nagendar, P. Jayaprakash, P. R. Krishna, K. V. S. Ramakrishna, A. C. Kunwar, *Angew. Chem., Int. Ed.* **2005**, *44*, 5878.
[12] M. A. Schmitt, S. H. Choi, I. A. Guzei, S. H. Gellman, *J. Am. Chem. Soc.* **2006**, *128*, 4538.
[13] R. L. Baldwin, *J. Mol. Biol.* **2007**, *371*, 283.
[14] D. Seebach, J. L. Matthews, *Chem. Commun.* **1997**, *79*, 2015.
[15] K. Gademann, T. Hintermann, J. V. Schreiber, *Curr. Med. Chem.* **1999**, *6*, 905.
[16] A. Glättli, D. Seebach, W. F. van Gunsteren, *Helv. Chim. Acta* **2004**, *87*, 2487.
[17] Z. Gattin, W. F. van Gunsteren, *J. Phys. Chem. B* **2009**, *113*, 8695.
[18] B. Keller, Z. Gattin, W. F. van Gunsteren, *Proteins* **2010**, in press.
[19] R. I. Mathad, B. Jaun, O. Flögel, J. Gardiner, M. Löweneck, J. D. C. Codée, P. H. Seeberger, D. Seebach, M. K. Edmonds, F. H. M. Graichen, A. D. Abell, *Helv. Chim. Acta* **2007**, *90*, 2251.
[20] W. F. van Gunsteren, S. R. Billeter, A. A. Eising, P. H. Hünenberger, P. Krüger, A. E. Mark, W. R. P. Scott, I. G. Tironi, 'Biomolecular Simulation: The GROMOS96 Manual and User Guide', vdf Hochschulverlag AG an der ETH Zürich, 1996.
[21] W. R. P. Scott, P. H. Hünenberger, I. G. Tironi, A. E. Mark, S. R. Billeter, J. Fennen, A. E. Torda, T. Huber, P. Krüger, W. F. van Gunsteren, *J. Phys. Chem. A* **1999**, *103*, 3596.
[22] C. Oostenbrink, A. Villa, A. E. Mark, W. F. van Gunsteren, *J. Comput. Chem.* **2004**, *25*, 1656.
[23] M. Fioroni, K. Burger, A. E. Mark, D. Roccatano, *J. Phys. Chem. B* **2001**, *105*, 10967.
[24] R. Walser, A. E. Mark, W. F. van Gunsteren, M. Lauterbach, G. Wipff, *J. Chem. Phys.* **2000**, *112*, 10450.
[25] J.-P. Ryckaert, G. Ciccotti, H. J. C. Berendsen, *J. Comput. Phys.* **1977**, *23*, 327.
[26] J. A. Barker, R. O. Watts, *Mol. Phys.* **1973**, *26*, 789.
[27] I. G. Tironi, R. Sperb, P. E. Smith, W. F. van Gunsteren, *J. Chem. Phys.* **1995**, *102*, 5451.
[28] H. J. C. Berendsen, J. P. M. Postma, W. F. van Gunsteren, A. DiNola, J. R. Haak, *J. Chem. Phys.* **1984**, *81*, 3684.
[29] M. Christen, B. Keller, W. F. van Gunsteren, *J. Biomol. NMR* **2007**, *39*, 265.
[30] J. A. Allison, W. F. van Gunsteren, *ChemPhysChem* **2009**, *10*, 3213.
[31] R. Kaptein, E. R. P. Zuiderweg, R. M. Scheek, R. Boelens, W. F. van Gunsteren, *J. Mol. Biol.* **1985**, *182*, 179.
[32] A. E. Torda, R. M. Scheek, W. F. van Gunsteren, *J. Mol. Biol.* **1990**, *214*, 223.
[33] Z. Gattin, A. Glättli, B. Jaun, W. F. van Gunsteren, *Biopolymers* **2007**, *85*, 318.
[34] X. Daura, W. F. van Gunsteren, A. E. Mark, *Proteins* **1999**, *34*, 269.
[35] K. Wüthrich, M. Billeter, W. Braun, *J. Mol. Biol.* **1983**, *169*, 949.
[36] M. Karplus, *J. Chem. Phys.* **1959**, *30*, 11.
[37] M. Karplus, *J. Am. Chem. Soc.* **1963**, *85*, 2870.
[38] A. Pardi, M. Billeter, K. Wüthrich, *J. Mol. Biol.* **1984**, *180*, 741.
[39] D. Wang, B. Jaun, W. F. van Gunsteren, *ChemBioChem* **2009**, *10*, 2032.

Received May 4, 2010